université paris — sud
INSTITUT DE PHYSIQUE NUCLEAIRE
B.P. N° 1 — 91406 ORSAY — TEL. 941.51.10
laboratoire associé à l'IN2P3

EXCITATION FUNCTIONS FOR QUASI-ELASTIC TRANSFER REACTIONS INDUCED WITH HEAVY IONS IN BISMUTH

D. GARDES, R. BIMBOT, J. MAISON,
L. de REILHAC, M.F. RIVET

and

A. FLEURY, F. HUBERT, Y. LLABADOR,

C.E.N. Bordeaux Gradignan

IPNO RC 77-10

Excitation Functions for Quasi-Elastic Transfer Reactions induced with Heavy Ions in Bismuth

D.Gardès, R.Bimbot, J. Maison, L.de Railhac, M.F.Rivet

Institut de Physique Nucléaire, Laboratoire de Chimie Nucléaire,

BP n°1, 91406.Orsay, France

and

A.Fleury, F.Hubert, Y.Llabador,

C.E.N. Bordeaux Gradignan

Laboratoire de Chimie Nucléaire ERA n°144

Le Haut-Vigneau, 33170 Gradignan, France

Abstract.

The excitation functions for the production of ^{210}Bi, ^{210}Po, $^{207-211}At$ and ^{211}Rn through quasi-elastic transfer reactions induced with heavy ions in ^{209}Bi have been measured. The corresponding reactions involved the transfer of one neutron, one proton, two and three charges from projectile to target. The projectiles used were ^{12}C, ^{14}N, ^{16}O, ^{19}F, ^{20}Ne, ^{40}Ar, ^{40}Ca, ^{56}Fe and ^{63}Cu.

The experimental techniques involved target irradiations and off-line α and γ activity measurements. Chemical separations were used to solve specific problems. Careful measurements of incident energies and cross sections were performed close to the reaction thresholds.

All excitation functions exhibit the typical features of quasi-elastic transfer reactions : a sharp increase at low energy, and a constant value at high incident energy. The position of the thresholds are

strongly influenced by the energetics of the reaction : high cross sections are observed under the strong interaction barrier if the energy balance at the minimum distance of approach is positive. This balance is equal to the difference between the interaction potentials in the entrance and exit channels, corrected for the mass balance. The constant cross sections observed for the high energy part of a given excitation function are consistent with the assumption that the curve P(R) which represents the transfer probability versus the distance between the nucleus centers does not vary with incident energy. This assumption implies the constancy of the optimum distance of approach R_{opt}, of the R window ΔR for which P(R) is significant, and of the magnitude of P(R).

Moreover the data show that the high energy cross sections for one-proton transfer are independent of the projectile, while odd-even effects of the projectile atomic number Z on the two-charge transfer cross sections are observed for the lightest incident ions ^{14}N to ^{20}Ne.

1. Introduction

Quasi-elastic transfer reactions induced with heavy ions have been extensively studied (see the review papers[1-3]). Two classes of experimental techniques have been used, based on the detection either of the light or of the heavy reaction product. The energy and angular distribution of the projectile residue can be accurately determined, using solid-state detectors, and such measurements were used for reaction mechanism as well as for nuclear structure studies[4-6]. The heavy target residues are generally collected using recoil techniques and unambiguously identified by their radioactive decay properties (type of decay, energy, half-

life). Such techniques are particularly fruitful for measuring absolute cross sections, and for systematic studies in which large numbers of data must be gathered. Recoil techniques give additional information on the kinematics of the reaction[7-12].

The large variety of heavy ions, from ^{12}C to ^{84}Kr, available at the ALICE Orsay Accelerator made it possible to undertake an extensive study of quasi-elastic transfer reactions. In this study, the target was chosen to be ^{209}Bi, and the observed nuclei were ^{210}Po, various isotopes of At and ^{211}Rn. The corresponding reactions involved the capture of one, two and three charges respectively by the target. The experimental data, part of which have been already published[13-15], included absolute cross sections, projected ranges along the beam axis, angular distributions and range distributions for each laboratory angle.

The kinematic information were used to transform the data into the c.m. system and to determine the reaction channels leading to the observed nuclei .

In the measurement of absolute cross sections, special care was taken to determine accurately the excitation functions close to their thresholds. The influence of the reaction energetics on the position of these energy thresholds was shown in ref.[16].

This paper presents a set of experimental results concerning excitation functions induced with ^{12}C, ^{14}N, ^{16}O, ^{19}F, ^{20}Ne, ^{40}Ar, ^{40}Ca, ^{56}Fe and ^{63}Cu. After a short description of the experimental techniques in section II, the results will be given in section III. In section IV, the typical features of transfer excitation functions will be discussed: general shape of the curves, position of the thresholds relative to the

calculated strong interaction barrier, and constant value of the cross section for high incident energies. As far as two-charge transfer reactions are concerned, an odd-even effect of the atomic number of the projectile on high-energy cross sections has been observed and this effect is also discussed in section IV.

Subsequent papers will give the experimental data concerning projected ranges and angular distributions, quantitative interpretation of the excitation functions at low incident energy, and of the angular distributions.

II. Experimental techniques

II.1. General procedure

Beams of ^{12}C, ^{14}N, ^{16}O, ^{19}F, ^{20}Ne, ^{40}Ar, ^{40}Ca, ^{56}Fe and ^{63}Cu were accelerated by the Orsay ALICE facility. Projectiles of ^{19}F from the Orsay Tandem MP Van de Graaff accelerator were also used. The absolute cross sections were measured using activation techniques, the targets being placed in a Faraday cup. According to the incident beam and energy, a single target or a stack of targets were used. The incident energy was varied either by changing the acceleration parameters, or by using Al degradors[17].

For the projectiles from ^{19}F to ^{63}Cu, several Al catcher foils were used to stop the recoiling nuclei, and thus the projected ranges along the beam axis of the α-emitters could be measured simultaneously. The α and γ-activities of the catcher foils and targets were counted off-line using 2π-ionization chambers (for α-emitters) and Ge-Li detectors (for γ-emitters). The reaction products were thus identified by the energy

of the emitted particle and the decay half-life (see table 1).

Details on the experimental procedure are given in refs.13-15.

Chemical separations of At and Po by spontaneous deposition onto Ag foils were sometimes used to improve the sensitivity of the detection.

II.2. Problems associated with the decay of radioactive parents

Due to the decay of radioactive parents during the time elapsed between irradiation and counting, the measured cross sections could correspond to cumulative yields. Two types of experiments were performed in order to estimate the contribution of such parent decays to the observed cross section :

As far as ^{210}Po was concerned, the possible production from ^{210}At and ^{210}Bi, had to be considered, according to the following scheme

$$^{210}\text{At} \xrightarrow{\text{E.C.}} {}^{210}\text{Po} \xleftarrow{\beta^-} {}^{210}\text{Bi}$$
(8.3h) (138d) (5d)

The cross section for ^{210}At production was directly measured by its γ-ray emission (Table 1). That for ^{210}Bi (or its upper limit) was measured in some experiments by the following technique : forty-eight hours after the irradiation, the target and catcher foils were dissolved and ^{210}Po was extracted by spontaneous deposition on silver. Several extractions were performed in order to remove 99% of the α-activity from the solution. This activity included the contribution from ^{210}At decay, but ^{210}Bi remained in the solution. Six days later, a second series of extractions of ^{210}Po were performed in order to collect the α-activity accumulated from ^{210}Bi decay. The sensitivity of this procedure was such that the ^{210}Bi

production cross section could be measured even if the ^{210}Po cross section was 100 times higher.

As far as ^{211}At was concerned, the possible contributions of ^{211}Rn and ^{215}Fr decays had to be considered, according to the following scheme :

$$^{211}Rn \xrightarrow[74\%]{E.C.} {}^{211}At \xleftarrow{\alpha} {}^{215}Fr$$
$$(14.6h) \qquad (7.2h) \qquad (0.5\mu s)$$

The cross section for ^{211}Rn production was deduced from the analysis of the ^{211}At decay curve[13]. The ^{215}Fr production, which involves the transfer of at least 4 charges from projectile to target, was estimated either from the analysis of the angular and energy distributions of residual nuclei[14] or from the measurement of the cross sections for the same reactions induced in targets of ^{197}Au [14], or ^{205}Tl [15]. The cross sections for the reactions ^{19}F, ^{20}Ne, $^{40}Ar + {}^{205}Tl \rightarrow {}^{211}At$, ^{211}Rn are given in table 11.

From these results, it can be deduced that the 4-charge transfer contribution to the ^{211}At formation can be always neglected relatively to that of 2-charge transfer reactions, with an important exception for incident ^{12}C (see ref.14).

II.3. Low energy part of the excitation functions

Special care was taken to determine accurately the lowest energy parts of the excitation functions.

Incident energy measurements

The energy of the ^{19}F beam from the Tandem was measured with an accuracy better than 0.1% using a deflection magnet. The energy of the ions accelerated with ALICE could be calculated with an uncertainty of

± 3% by the relation

$$E_c(\text{MeV}) = \frac{F^2 R^2}{4,84} \cdot A \qquad (1)$$

in which F(MHz) is the cyclotron high frequency value, R(m) the extraction radius, and A(uma) the mass of the ion.

In order to improve the precision on the incident enorgy determination particularly at energies close to the reaction thresholds, a system of the type described by O.K.Olsen et al.[24] was used. The principle of the method is to measure, with a solid state detector, the energy of protons elastically scattered at 0° from a formvar target, the beam being stopped in a gold foil in which the protons loose only a few percent of their energy. This method can be applied to heavy ions up to 6 MeV per nucleon. The precision on the absolute energy value is equal to about ± 0.5%.

This method was also used to study the applicability of relation (1). This study[25] showed a systematic deviation, the measured energy being equal to

$$E_m(\text{MeV}) = 0.987\ E_c - 0.3 \qquad (2)$$

This last expression, associated with an uncertainty of ± 2% was adopted for incident energy whenever no measurement was made.

Secondary reactions

The nuclear reactions induced by the incident beam in the target, its Al backing, or Al degradors produce a secondary flux of light particles, such as protons and α-particles. These particles can induce in the target nuclear reactions which produce the same isotope as the studied transfer reactions :

$$p + {}^{209}Bi \rightarrow {}^{210}Po \qquad \text{or}$$
$$\alpha + {}^{209}Bi \rightarrow {}^{211}At + 2n$$

This "secondary" production is generally negligible relatively to the transfer cross sections. However, if a stack of degradors are used, this production may correspond to an apparent cross section as large as 10-50 µb and even be higher than that of the transfer reaction close to the threshold. This difficulty can be removed

i) by avoiding the use of a stack of degradors for these low energy measurements. This is necessary anyway to get a good definition of the incident energy.

ii) by selecting for the counting the catcher foils which correspond to projected ranges larger than 0.2 mg/cm^2 of aluminium. Indeed the ranges of transfer reaction products in Al are of the order of 1-2 mg/cm^2 for their threshold energies, while those of secondary products are typically of 0.1 mg/cm^2.

Spurious beams

In the case of ^{40}Ca projectiles, a sub-coulomb maximum was first observed in the excitation functions. A careful study showed that this maximum was due to the presence of a slight contamination in the ^{40}Ca beam by ^{40}Ar ions. In subsequent experiments, the purity of the ^{40}Ca beam was controlled by a technique in which a thick Al foil is irradiated, and the activity of ^{41}Ar is measured (E_γ = 1.2936 MeV, T = 1.83h). The cross section for the production of this isotope being very small with ^{40}Ca projectiles, and much larger with ^{40}Ar ions, the method is sensitive to a 1% ^{40}Ar contamination.

III. Experimental results

The experimental cross sections for the production of the observed residual nuclei through reactions induced with ^{12}C to ^{63}Cu in ^{209}Bi targets are given in tables 2 to 11. For the incident ions ^{12}C and ^{40}Ar, some of these data had been already published[13,14], but in this work the measurements were extended to other incident energies and/or other transfer products. Moreover, for the ^{40}Ar induced reactions, small corrections were applied on the energy or cross section values. Energy corrections were due to the application of relation (2), and cross section correction to a better calculation of self absorption of the emitted α-particles in the catcher foils (instead of assuming an average depth for the radioactive nuclei, the calculation takes into account the distribution of these nuclei in the catcher foil).

As was mentionned in sect.II, the experimental values obtained for ^{210}Po include the contributions of ^{210}At and ^{210}Bi. They are labelled ^{210}(Po+At+Bi) in tables 2-11. Whenever it was possible, the contribution of ^{210}At and eventually of ^{210}Bi was subtracted to these cumulative values, and the resulting cross sections are also quoted in the tables. In order to reduce the uncertainties, the values adopted for $\sigma(^{210}At)$ and $\sigma(^{210}Bi)$ in these subtractions were taken from a curve fitting the experimental excitation functions. Therefore, they may be slightly different from the corresponding cross sections found in the same lines of the tables.

The energy values quoted in the tables correspond to the mid-plane of the targets. The uncertainties associated with these values include the errors on the energy of the incident beam (discussed in sect.II), and the uncertainties on the energy losses in the Al degradors

This last error was estimated to ± 15% of the energy loss. The uncertainties on cross sections take into account the errors on beam flux measurements (± 2%), target thickness and homogeneity (± 5%), counting efficiencies (± 2-10% for α-counting, ± 4% for γ-detectors), branching ratios (± 5-10% for γ-emitters), and the statistical errors on activities (± 5-50%).

The experimental excitation functions are presented in figs.1 to 13. In order to make the presentation clearer, most of the uncertainties on incident energies are not shown in these figures. Moreover, solid lines have been drawn to guide the eye through the experimental points. In figs.8 and 12, a higher weight has been given for drawing these lines to the point for which the incident energy is accurately known. A vertical arrow indicates the value of the strong interaction barrier B, defined as the energy for which the interaction potential of the system at zero angular momentum is maximum[26], and calculated according to the energy density formalism[27].

For each projectile, the curves relative to ^{210}Po and ^{211}At, corresponding respectively to the net gain of one and two protons by the target, can be compared in figs.1,2,3,5,..,8,10,12. The excitation functions of At isotopes, corresponding to a net gain of 2 charges by the target, are shown in figs.2,4,7,9,11,13. In fig.2, the results from the present work are compared to those from Croft et al.[10]. A good agreement is observed at high incident energy, but close to the reaction threshold, the values from ref.10 are much higher. It has been pointed out in section II that secondary reactions could increase significantly the measured cross sections in this energy region. Such effects might explain the high values found in ref.10.

All the curves in figs.1-13 exhibit a typical shape commonly

observed for quasi-elastic transfer reaction excitation functions : the cross sections increase rapidly at low incident energies, and become nearly constant at high energies[3,7-13]. A detailed discussion of these experimental results is given in the next section.

IV. Discussion

IV.1. Introductory remarks

First, it should be noted that, as was already mentionned in several papers[10-15,39] the identification of a given residual nucleus is generally not sufficient to specify unambiguously the reaction involves in creating it. The various processes leading from the target to the observed nucleus can be denoted by expressions of the type (+A,B), in which the symbol A represents the nucleons transferred in the direct process, with the sign + for transfers from projectile to target, and B the particles emitted in the subsequent de-excitation by the target residue. For example, the reaction $^{209}Bi + H.I. \rightarrow {}^{211}At$ may be due to the (+2p,γ), (+2p+n,n), (+α,2n) processes. As was shown in section II, the contribution of 4-charge transfers leading to ^{215}Fr which decays through α-emission can be neglected for all projectiles but ^{12}C. As far as light projectiles are concerned, kinematic analysis of the c.m. energy distributions relative to the heavy product were performed, and used to distinguish between the reaction channels involving two-charge transfers[14,28,29]. But even when this analysis makes it possible to assign a definite reaction channel, such as (+2p,γ), this notation includes a variety of elementary transfer reactions, each of them leading to a well-defined level in the exit channel.

For all these reasons, a given experimental excitation function

has to be considered as the sum of many contributions.

The second remark concerns the experimental cross sections for ^{210}Po production : except for low energy ^{16}O, this cross section is always higher than that for At isotopes production. This property may be related to the fact that the simplest process involved in ^{210}Po production is a single proton transfer, whereas the production of any At isotope requires the transfer of at least two protons, generally less probable. The exception observed for the reaction $^{16}O+^{209}Bi$ at low energy will be discussed in subsect.IV.2.

It can be seen in tables 2-4 that the ^{210}Po cross section is also higher than that for ^{210}Bi production, which involves one-neutron transfer, whenever it has been measured. This can be explained by the fact that ^{210}Bi production is reduced i) by unfavourable energetics (see table 12), ii) by the presence of a long-lived isomer ^{210m}Bi (268 keV, $T = 3.10^6 Y$) which cannot be measured here, and which acts as a shielding. Therefore, the ^{210}Bi production is only due to the direct transfer towards the groundstate. However, one should note that low cross sections are also observed[30] for the reactions ^{12}C, ^{14}N, $^{16}O+^{197}Au \rightarrow ^{198}Au$ although no shielding effect can be attributed to any isomer of ^{198}Au.

The third remark concerns the thresholds of the different reactions. The position of these thresholds, which can be compared to each other and to the calculated strong interaction barrier B, showed by an arrow in figs.1-13, depends strongly on the incident ion, and on the reaction involved. This fact, which can be related to the reaction energetics, will be discussed in subsect.IV.2. It is clear from the results however that the barrier B cannot be considered as a reaction threshold, since many reactions occur with significant cross sections below this barrier.

Finally, a striking feature of the transfer excitation functions is the leveling-off of the cross sections for a given reaction at high incident energy. Moreover, the comparison of the data obtained with several projectiles indicate that

i) as far as ^{210}Po is concerned, the cross sections observed for the excitation functions "plateaus" seem to be independent of the projectile.

ii) for the At isotopes, an influence of the parity of the projectile Z on these values is observed for light projectiles. These aspects will be discussed in subsection IV.3.

IV.2. Low-energy cross sections - Influence of the reaction energetics

IV.2.1. Excitation functions of ^{210}Po and ^{211}At.

The kinematic analysis mentionned in subsect.IV.1 showed that the production of ^{210}Po and ^{211}At at low energy could be attributed for all projectiles lighter than ^{40}Ar, to the processes (p,γ) and (2p,γ) respectively[29]. For the heaviest projectiles (^{40}Ar to ^{63}Cu), this analysis was not precise enough, and the assumption was made that these processes are still the most probable at low energy. Therefore, the following discussion of the reaction thresholds will be made under this assumption for all projectiles.

It can be remarked in figs.1-3,5,6,8,10,12, that the positions of the ^{210}Po and ^{211}At excitation functions relatively to each other and to the calculated barrier depend strongly on the incident ion. This effect was discussed in ref.16 in terms of the relative positions of the curves $V_i(R)$ and $V_f(R) - Q_{gg}$. The terms $V_i(R)$ and $V_f(R)$ denote the variation of the interaction potential of the system (sum of the coulomb and nuclear potentials) in the entrance and exit channels at zero angular

momentum, versus the distance R between the nucleus center. The term Q_{gg} is the mass balance in the reaction.

When the curve $V_i(R)$ is situated above the curve $V_f(R) - Q_{gg}$, $(V_i(R) > V_f(R) - Q_{gg})$, the energetics favors the transfer reaction which can take place if the incident energy allows sufficient overlap of the nuclear matter. If $V_i(R) < V_f(R) - Q_{gg}$, the transfer reaction is energetically forbidden.

In fig.14, are shown the potential energy curves corresponding to the entrance channels and to the system after 1p and 2p-transfer for seven projectiles. These curves were calculated using the following expression[27] for the interaction potential V(R) :

$$V(R) = V_c(R) + V_N(R) \quad (3) \qquad \text{with}$$

$$V_c(R) = Z_1 Z_2 e^2/R \quad (4) \qquad \text{and}$$

$$V_N(R) = -30 \exp\left[-0.27(R - r_o[A_1^{1/3}+A_2^{1/3}])^2\right] \quad (5)$$

with $r_o = 1$ fm.

A_1, Z_1 and A_2, Z_2 being the projectile and target masses and charges.

Two situations can be encountered :

Situation (1) : the curve corresponding to the exit channel is situated under that corresponding to the entrance channel for all distances R such that a sufficient overlap of nuclear matter can take place (e.g. $R \lesssim 20$ fm). This situation is correlated with the observation of high sub barrier cross sections.

Situation (2) : the curves corresponding to the entrance and exit channels cross for a R value situation in the region of interest ($R \lesssim 20$ fm). This crossing point plays the role of an energy threshold, and the experimental thresholds observed are close to the strong interaction barrier (maximum value of $V_i(R)$).

As was stated in ref.16, these energetic situations can be summarized by the value of the expression $Q_{gg} - \Delta B$, ΔB being the difference between the maxima of the interaction potentials in the entrance and exit channels. A high positive value of this expression corresponds to favourable energetics. These values are given in table 12 for the reactions studied, and it can be seen that, for ^{210}Po and ^{211}At productions, the $Q_{gg} - \Delta B$ values are always positive, but vary from 0.1 MeV to 8.3 MeV.

It can be checked from the experimental data that correlations between the potential energy curves (or the $Q_{gg}-\Delta B$ values) and the excitation functions are always observed. Interesting comparisons can be made :

i) between the three light systems, N, O, F+Bi, the one-proton transfer being favoured by the energetics for odd-Z projectiles.This result extends the comparison already made in ref.16 for ^{14}N and ^{16}O.

ii) between the ^{40}Ar+Bi and ^{40}Ca+Bi systems corresponding to the same incident mass, but much different energetics, the Ca-induced reactions being strongly favoured. Their thresholds are situated well below the barrier while the cross sections for Ar-induced reactions, less favoured, become significant for incident energies much closer to the barrier.

iii) between the ^{56}Fe+Bi and ^{63}Cu+Bi systems, the former corresponding to an energetic situation slightly more favourable than that of the ^{40}Ar+Bi system, and the latter to a situation equivalent to that of the ^{40}Ca+Bi system for 1p transfer, and less favourable but still good for 2p transfer reactions. The excitation functions in figs.10 and 12 reflect well these energetic situations.

A quantitative study of the reactions close to the threshold is presented in ref.29.

IV.2.2. Excitation functions of other At isotopes

It can be seen in figs.2 and 3 that, for ^{16}O and ^{19}F projectiles, the thresholds for ^{210}At production are situated about 10 MeV higher than those for ^{211}At, and slightly above the calculated barrier. On the other hand, for heavier projectiles, ^{210}At and even ^{209}At, are produced with significant cross sections below the barrier (figs.7,9,11,13). In order to understand this experimental observation, it is first necessary to discuss the nature of the reactions producing the observed isotopes.

As far as ^{210}At is concerned, two processes must be considered.

i) the direct transfer of 2 protons towards target and one neutron towards projectile, producing an ^{210}At nucleus with little excitation energy, process denoted (+2p-n,γ).

ii) the transfer of 2 protons leading to an excited ^{211}At which evaporates one neutron (process +2p,n). The minimum excitation energy involved for the intermediate nucleus ^{211}At is then $E^*_{min} \simeq 7$ MeV.

As far as ^{209}At is concerned, the reactions (+2p-2n,γ), (+2p-n,n), (+2p,2n) have to be considered, with $E^*_{min} = 0, 7, 15.7$ MeV respectively. The values of the expression $Q - \Delta B$, in which $-Q = E^*_{min} - Q_{gg}$ is the minimum energy absorbed in the reaction, are given in Table 12 for the reactions considered. Considering the values of table 12 and the experimental data, it can be concluded that the observation of significant sub barrier cross sections for the production of a given isotope is correlated to the existence of at least one reaction for which the expression $Q - \Delta B$ is positive. One exception must be mentionned for the reaction $^{40}Ar + Bi \rightarrow ^{210}At$ for which a slightly negative value is found (the uncertainties involved in the calculation of ΔB might be responsible for this negative value).

This correlation seems to indicate that, for projectile from ^{40}Ar to ^{63}Cu at low energies, the reactions (+2p-n,γ) and (+2p-2n,γ) are those which produce ^{210}At and ^{209}At. These reactions involve the transfer of 3 and 4 nucleons respectively. The observation of significant cross sections for these reactions are in good agreement with other experimental data[32] which indicate that multi-nucleon transfers have an increasing probability at barrier energies when the mass of the projectile is increased.

IV.2.3. Excitation function of ^{211}Rn

Except for ^{14}N ions, no ^{211}Rn production is observed close to the barrier for the light projectiles. As far as this last ion is concerned, the range measurements and angular distributions have shwon[29,31] that the production of ^{211}Rn is due to the compound nucleus reaction $^{14}N + ^{209}Bi \rightarrow ^{219}Th + 4n$, followed by fast α decays of ^{219}Th and ^{215}Fr.

For Ar projectiles, the threshold of the excitation function is slightly higher than the barrier ; for heavier projectiles, the thresholds are lower than the barrier. These results can be explained by the values of $Q - \Delta B$ quoted in table 12, the production of ^{211}Rn being mainly due to the process (+3p-n,γ) for all projectiles, with a possible contribution of the reaction (+3p,n) for incident ^{40}Ca.

IV.3. High energy cross sections

IV.3.1. Influence of incident energy for a given reaction

The cross section for a given transfer reaction can be calculated by the formula :

$$\sigma(\bar{E}) = \pi \lambda^2 \sum_{\ell=0}^{\infty} (2\ell+1)\, P(\ell) \qquad (6)$$

In this expression, $\bar{E}$ denotes the c.m. incident energy, λ the de Broglie wave length, ℓ the angular momentum, and $P(\ell)$ the transfer probability for the partial wave ℓ . As was already mentionned by Frahn and Venter[33], the small variation of the cross section versus incident energy, in the high-energy parts of the excitation functions can be interpreted under the following assumptions :

i) the transfer probability is maximum for an optimum distance of approach :

$$R_{opt} = r_0\left(A_1^{1/3} + A_2^{1/3}\right) \qquad (7)$$

the parameter r_0 being independent of $\bar{E}$ for the high energies considered. This current assumption[3,33,34] is used to calculate the angular momentum value ℓ_{opt} which corresponds to the maximum of $P(\ell)$.

ii) the range ΔR of R values for which the transfer probability is significant is also constant. It can be seen on fig.15 that, for sufficiently high incident energies ($E \geq 100$ MeV), this hypothesis is about equivalent to the assumption of a constant width $\Delta\ell$ of the angular momentum window, since the curves $R = f(\ell)$ corresponding to various values of the incident energy are well approximated by parallel straight lines. The curves given in fig.15 have been obtained from the equation $\ell = R\{2\mu[\bar{E} - V(R)]\}^{1/2}$ (8), in which μ is the reduced mass. Assumptions i) and ii) are in good agreement with the results of angular distribution analysis[29,33].

iii) the shape and amplitude of the distribution $P(\ell)$ are independent of incident energy. When this energy is varied, only the value of ℓ_{opt} is varied.

The calculation of $\sigma(E)$ was performed for the system $^{19}F+Bi$ according to these assumptions, with $r_0 = 1.5$ fm, $\Delta R = 1.5$ fm, and for two different shapes of the distribution $P(\ell)$:

- Square distribution : $P(\ell) = k$ for $\ell_1 \leq \ell \leq \ell_2$

$P(\ell) = 0$ for $\ell < \ell_1$, $\ell > \ell_2$

with $\ell_1 = \ell_{opt} - \frac{\Delta\ell}{2}$, $\ell_2 = \ell_{opt} + \frac{\Delta\ell}{2}$.

Expression (6) can then be written under the form

$$\sigma(\bar{E}) = k \cdot \pi\lambda^2 \sum_{\ell=\ell_1}^{\ell_2} (2\ell+1) \qquad (9)$$

and the variation of σ is obviously reduced to the variation of a geometrical term.

- Gaussian distribution :

$$P(\ell) = P(\ell_{opt}) \exp\left[-\frac{(\ell-\ell_{opt})^2}{2\Lambda^2}\right] \qquad (10)$$

with $\Lambda = \Delta\ell/2\sqrt{2 \log 2}$

The results of these calculations are given in fig.18, and compared to the experimental points, after arbitrary normalisation of the calculated curve. It can be seen that both distributions lead to a fairly good representation of the high energy part of the excitation functions.

This agreement must be taken as a confirmation of the validity of assumption iii) which expresses as a first order approximation the constancy of the transfer probability at high energy. This constancy may seem to be contradictory with the well known dependence of optimum Q-values on the incident energies[35]

$$Q_{opt}(\bar{E}) = \frac{Z_3Z_4 - Z_1Z_2}{Z_1Z_2}\ \bar{E} \qquad (11)$$

Z_3 and Z_4 being the atomic number of the nuclei after transfer, and $\bar{E}$ the incident energy in the c.m. system. The excitation function for a reaction corresponding to a given Q-value Q_o should exhibit a maximum for the incident energy $\bar{E}_o$ such that $Q_{opt}(\bar{E}_o) = Q_o$.

One must remember, however, that the observed excitation functions represent the sum over several reactions, as was outlined in subsection IV.1., and experimentally shown in ref.14 for $^{12}C+^{81}Bi$ reactions. Moreover, each of these reactions leads to a high number of levels. Therefore, a quasi-continuum of Q-values have to be considered, and the constancy of the transfer probability must be understood as being due to the summation over all the exit channels. This interpretation is confirmed by the different shapes observed for the excitation functions when the number of possible reactions is reduced, either by the high fissionability of the produced nuclei, as in ref.36, or by a selection based on the energetics of the reaction, as in ref.14. Then, a broad maximum is effectively observed in the excitation function. Such maxima have also been obtained in calculated excitation functions for well defined transfer reactions[37], i.e. when limits have been set for the possible variations of Q.

IV.3.2. Influence of the projectile

In fig.17, the cross sections corresponding to the excitation function "plateaus" are plotted versus the atomic number of the projectile

i) for ^{210}Po production (1p transfer)

ii) for ^{211}At production (2p transfer)

iii) for the sum of At isotopes (2 charge transfer).

It can be seen that the 1p transfer cross sections lie in the range 60-80 mb for all projectiles. This constant value observed for reactions which correspond to different Q_{gg}-ΔQ values (see table 12) seem to indicate that this energetic parameter has little influence at high incident energies. This may be understood by the fact that this parameter is calculated on the assumption of ℓ=0 incident waves and ground-state-ground-state transitions. These conditions which correspond roughly to the low energy reactions are certainly not fulfilled for high incident energies and the possibility of angular momentum transfer, associated with the large number of possible reactions and available excited levels smears out the energetic effects.

On the other hand, however, it can be seen in fig.17, that the cross sections corresponding to ^{211}At production, and to the sum of At isotopes exhibit an odd-even effect for light projectiles. This effect is strong for Z=7, somewhat reduced for Z=9, and vanishes for Z=29. These results indicate that the 2-proton transfer probability may be enhanced if the projectile structure is such that pairs of protons are present close to its surface. Such effects have been already mentionned by Von Oertzen[38] for one and two-proton transfer reactions induced by ^{16}O on ^{144}Sm.

V. Conclusion

The excitation functions observed for quasi-elastic transfer reactions are characterized by two main features : a sharp increase of the cross sections at low incident energies, and a high-energy plateau. These two features can be explained by the influence of two simple physical concepts, that of optimum distance of approach for transfer, and that of energy balance of the reaction at the distance of approach where the

transfer occurs. The energetic aspect dominates for low incident energies, the geometrical one for high incident energies.

For one and two-proton reactions leading to ^{210}Po and ^{211}At, the position of the excitation function thresholds relative to the strong interaction barrier are mostly influenced by the relative positions of the potential energy curves corresponding to the ground state in the entrance and exit channels. For positive values of the difference $Q_{gg}-\Delta B$, significant sub-barrier cross sections can be observed. The results relative to the more complex reactions leading to $^{207-210}At$ isotopes and to ^{211}Rn indicate that these reactions can be observed at energies close to the interaction barrier if one of the possible reaction channels corresponds to a positive value of $Q-\Delta B$. This reaction channel is always the one which leads to the smallest excitation of the nuclei (0-7 MeV).Therefore the term quasi-elastic can still be used for these reactions. Quasi-elastic transfers of up to 4 nucleons have thus been observed for the heaviest projectiles ($A_1 \geqslant 40$).

For high incident energies, the shapes of the excitation functions are dominated by the variation of the "geometrical" term $\pi\lambda^2 \sum_{\ell_1}^{\ell_2} (2\ell+1)$ versus incident energy, ℓ_1 and ℓ_2 being defined by the limits R_1 and R_2 of the distance of closest approach for which the transfer occurs, and these limits R_1 and R_2 being approximately independent of energy, for a given system target-projectile. This result indicates that the magnitude of the transfer probability $P(\ell)$ does not vary significantly with energy.

These features may be explained by the following considerations: for low incident energies, the threshold of the reaction is governed by the energetic possibility of the transfer towards the ground state levels

in the exit channel, i.e. by the value of Q_{gg}-ΔB. But as soon as this threshold energy is surpassed many levels become accessible, and for higher energies, the nuclear part of the interaction (i.e. the spectroscopic factors) will play a minor role for the type of reaction studied: the number of quantum states involved being fairly large, the absolute values of the cross sections will be sensitive to an average value of the spectroscopic factors. Moreover, for high incident energies, several reactions lead to the observed nuclei, and these reactions correspond to a continuum of Q-values. This contributes also to the smearing out of the energetics effects at these high incident energies.

The only effect of the projectile structure which remains, is an odd-even effect of the projectile atomic number Z_1 on two-charge transfer cross sections, the transfer probability being enhanced for even-Z projectiles.

Acknowledgements.

We want to thank the ALICE and Tandem crews for their cooperation, J.M.Alexander and M.Lefort for helpful discussions, and A.E.Vlieks for careful reading of the manuscript.

References

1 W.Von Oertzen, Nuclear Spectroscopy, J.Cerny ed. IV C.2 New York Academic

2 M.C.Lemaire, Physics Reports 7C, 279 (1973)

3 A.Fleury, J.M.Alexander, Ann. Rev.of Nucl. Science 24, 279 (1974).

4 J.Galin, D.Guerreau, M.Lefort, J.Péter, X.Tarrago, R.Bassile, Nucl. Phys. A159, 461 (1970)

5 J.L.C.Ford,Jr., K.S.Toth, G.R.Satchler, D.C.Hensley, L.W.Owen, R.M.DeVries, R.M.Gaedke, P.J.Riley, S.T.Thornton, Phys. Rev. C10, 1429 (1974)

6 P.R.Christensen, V.I.Manko, F.D.Becchetti, R.J.Nickles, Nucl. Phys. A207, 33 (1973)

7 J.M.Alexander, L.Winsberg, Phys. Rev. 121, 529 (1961)

8 H.Kumpf, E.D.Donetz, JETP 17, 539 (1963)

9 P.M.Strudler, I.L.Preiss, R.Wolfgang, Phys. Rev. 133B, 104 (1964)

10 P.D.Croft, K.Street Jr., Phys. Rev. 165, 1380 (1968)

11 R.L.Hahn, P.F.Dittner, K.S.Toth, O.L.Keller, Phys Rev. C10, 1889 (1974)

12 F.Hubert, H.Delagrange, A.Fleury, Nucl. Phys. A228, 415 (1974)

13 R.Bimbot, D.Gardès, M.F.Rivet, Phys. Rev. C4, 2180 (1971)

14 R.Bimbot, D.Gardès, M.F.Rivet, Nucl. Phys. A189, 193 (1972)

15 R.Bimbot, M.F.Rivet, Phys. Rev. C8, 375 (1973)

16 D.Gardès, R.Bimbot, A.Fleury, F.Hubert, M.F.Rivet, J. de Phys. Lettres 36, 59 (1975)

17 L.C.Northcliffe, R.F.Schilling, Nucl. Data Tables A7, 233 (1970)

18 C.M.Lederer, J.M.Hollander, I.Perlman, Table of Isotopes, Wiley and sons ed. N.Y. (1967)

19 I.Perlman, F.Asaro, A.Ghiorso, A.Larsh, R.Latimer, Phys. Rev. 127, 917 (1962)

20 S.Gueth et al., Dubna report P6, 4079 (1968)

21 G.Erdtmann and W.Soyka, Jül.-1003 - AC, (Sept.1973)

22 N.A.Golovkov et al., J.I.N.R. Dubna report P6, 4452 (1969)

23 E.F.Momyer, E.K.Hyde, J. Inorg. Nucl. Chem. 1, 274 (1955)

24 D.K.Olsen, N.H.Merrill, S.F.Biagi, N.R.Phillips, A.R.Barnett, Nucl. Inst. and Methods 114, 615 (1974)

25 R.Bimbot, S.Della Negra, D.Gardès, H.Gauvin,et B.Tamain, IPNO RC 77-03 (1977)

26 C.Y.Wong, Phys. Lett. 42B, 186 (1972) ; Phys. Lett. 31, 766 (1973)

27 C.Ngô, B.Tamain, J.Galin, M.Beiner, R.J.Lombard, Nucl. Phys. A240, 353 (1975)

28 J. Maison, (Thèse 3e cycle), Orsay (1972)

29 D.Gardès (Thèse) Orsay (1976)

30 R.Bimbot et al., unpublished data

31 D.Gardès et al., to be published

32 R.Bimbot,H.Gauvin,Y.Le Beyec,M.Lefort,N.T.Porile,B.Tamain,Nucl.Phys.A189, 539 (1972).

33 W.E.Frahn, R.H.Venter, Nucl. Phys. 59, 651 (1964)

34 J.A.McIntyre, T.L.Watts and F.C.Jobes, Phys. Rev. 119, 1331 (1960)

35 P.J.A.Buttle, L.J.B.Goldfarb, Nucl. Phys. A176, 225 (1971)

36 R.L.Hahn, P.F.Dittner, K.S.Toth, O.L.Keller, Phys. Rev. C10, 1889 (1974)

37 F.Hubert, Thèse, CEN Bordeaux Gradignan (1973)

38 W.Von Oertzen, H.G.Bohlen, G.Gebauer, Nucl. Phys. A207, 91 (1973)

39 S.Pandian, I.L.Preiss, Nucl. Phys. A282, 169 (1977).

Isotope	Half-life	Decay mode	E α or γ	Branching ratio	References
^{210}Po	138.4 d	α	5.305 MeV	1	18
^{211}Po	0.52 s	α	7.448 MeV	1	19
^{207}At	1.8 h	CE	814 keV	1	21
^{208}At	1.63 h	CE	685 keV	0.99	21
			860 keV	0.92	
^{209}At	5.42 h	α	5.66 MeV	0.041	20
		CE	782 keV	0.58	21
			545 keV	0.62	
^{210}At	8.3 h	CE	245 keV	0.79	21
			1180 keV	1	
^{211}At	7.2 h	α	5.868 MeV	0.409	22
^{210}Rn	2.42 h	α	6.04 MeV	0.96	23
^{211}Rn	16 h	α	5.85 MeV	0.26	23

Table 1

^{12}C	Cross sections (mb)					
E_{lab} (MeV)	^{211}At	^{210}At	^{209}At	^{210}Bi	$^{210}(Po+At+Bi)$	^{210}Po
88 ± 2	43 ± 9					
88 ± 2	46 ± 5	58 ± 6.5	63 ± 5			
87 ± 2	49 ± 10	48 ± 9	71 ± 11	0.8 ± 0.6	108 ± 30	54 ± 40
85 ± 2		61 ± 6	76.5 ± 6.5			
83.5 ± 2.5	44 ± 9					
82 ± 2.5	47 ± 9.5	36 ± 7	188 ± 38			
80.5 ± 3	39 ± 8					
79 ± 3	46.5 ± 9.3	38 ± 7	222 ± 35	1.5 ± 0.7	77 ± 20	33 ± 30
78 ± 3	39.2 ± 8					
76.5 ± 3	41.7 ± 8.4	51 ± 10	220 ± 37			
76 ± 3	40 ± 4	47 ± 5	221 ± 12			
75.5 ± 3.5	39.4 ± 8					
74 ± 3.5	42 ± 8.4	89 ± 18	137 ± 18	< 1.3	107 ± 40	< 20
73 ± 4		96 ± 11	149 ± 11			
71 ± 4	32.7 ± 6.6	111 ± 22	64 ± 9.5			
68.5 ± 4.5	26 ± 5.2	103 ± 20	5.2 ± 0.9	< 1.3	122 ± 45	< 20
65.5 ± 4.5	19.3 ± 4	51 ± 10	2.75 ± 0.65			
62.5 ± 5	5.2 ± 1	21 ± 4				

Table 2

^{14}N	cross sections (mb)			
E_{lab} (MeV)	^{211}At	^{211}Rn	^{210}Bi	$^{210}(Po+Bi)$
159 ± 3	11.4 ± 1.3	13.9 ± 2		80 ± 7
143 ± 5	12.2 ± 1.4	18.3 ± 2.7		62 ± 6
129 ± 7	13 ± 1.5	14.9 ± 2.2		72 ± 6.5
115 ± 9	10.4 ± 1.2	18.3 ± 2.7		62 ± 5.7
98 ± 2	11 ± 1.2	18.6 ± 2.7		52 ± 5
97 ± 2	11 ± 1.7	21.6 ± 3.4	8.7 ± 2.6	52 ± 12
94 ± 2	10 ± 1.6	15.8 ± 2.5		57 ± 12
91 ± 3	9.5 ± 1.5	10.7 ± 1.7	8 ± 2.4	47 ± 11
87 ± 3	7.7 ± 1.2	7.9 ± 1.2		49 ± 11
84 ± 3.5	5.4 ± 0.9	8.5 ± 1.5	3.6 ± 1.8	38 ± 8
81 ± 3.5	3.1 ± 0.5	6.3 ± 1		37 ± 8
77 ± 1.5	1.15 ± 0.18	1.3 ± 0.2	< 0.4	18 ± 3.6
73 ± 1.5	0.44 ± 0.06	0.66±0.09		19 ± 4
72 ± 2	0.08 ± 0.02	0.03±0.007		15 ± 3
69 ± 2	0.016±0.002	$(4.6\pm0.6)\times10^{-3}$		6.2±1.3
69 ± 2.5	$(4.4\pm1)\times10^{-3}$			5.1±1
66 ± 3	$(0.4\pm0.1)\times10^{-3}$			1.6±0.33
65 ± 3				0.6±1.2
61 ± 3.5	$(0.1\pm0.1)\times10^{-3}$			0.4±0.09

Table 3

^{16}O	cross sections (mb)				
$E_{(MeV)}$	^{211}At	^{210}At	^{210}Bi	$^{210}(Po+At+Bi)$	^{210}Po
99 ± 2.5	33 ± 4	22.6 ± 2.2	<2.8		
94 ± 3	34.5 ± 3.5	18.2 ± 1.6		69 ± 14	51 ± 15
88 ± 4	24 ± 3	6.8 ± 0.9	<1.5	64 ± 10	57 ± 11
83 ± 2	7.4 ± 1	0.24±0.12	<0.5	31 ± 9	31 ± 9
82 ± 2	6.3 ± 1			0.05±0.005	0.05±0.005
77 ± 5	0.1 ± 0.015			$(8\pm1)\times10^{-3}$	$(8\pm1)\times10^{-3}$
77 ± 2.5	0.05 ± 0.01				
72 ± 6	$(4\pm2)\times10^{-3}$				
67 ± 4	$(1.1\pm0.5)\times10^{-4}$				
63 ± 7	$(5\pm2.5)\times10^{-4}$				
62 ± 4	$(4\pm2)\times10^{-4}$				
58 ± 5	$(2.7\pm1.3)\times10^{-4}$				

Table 4

^{19}F	cross sections (mb)						
E_{lab} (MeV)	^{211}At	^{210}At	^{209}At	^{208}At	^{207}At	$^{210}(Po+At+Bi)$	$^{210}(Po+Bi)$
185.5 ± 3.7	23 ± 1.8	31.4±1	45 ± 7	16 ± 2	10 ± 5	128 ± 8	97 ± 9
185 ± 3.7	24.1 ± 2					151 ± 8.5	120 ± 9
169.5 ± 7	26.4 ± 2	31.6±1				155 ± 8.5	123 ± 9.5
151.5 ± 10	23 ± 1.8	24.6±3				110 ± 7	85 ± 10
132.5 ± 13	21.1 ± 1.7	17 ±4				98 ± 6	81 ± 10
119 ± 13	25.9 ± 2.1	12 ±1.5				101 ± 5.5	89 ± 7
109 ± 14	18.2 ± 1.5	7.5 ±0.9				79 ± 4	71.5 ± 5
109 ± 0.3	19 ± 3	4.2 ±0.2				76.6 ± 4	72.4 ± 4
104.5 ± 0.3	15.5 ± 1.7	2.9 ±0.2				70.7 ± 4	68 ± 4
99 ± 0.3	5 ± 0.4	0.51±0.15				32.3 ± 3	31.8 ± 3
94 ± 0.3	2.5 ± 0.3	0.16±0.13				26.5 ± 4	26.3 ± 4
91.5 ± 0.3	1.88 ± 0.26					31.3 ± 1.5	31.3 ± 1.5
89 ± 0.3	0.39 ± 0.04					14.7 ± 1.5	14.7 ± 1.5
87 ± 0.3	0.22 ± 0.04					15.7 ± 1.6	15.7 ± 1.6
83.7 ± 0.3	0.0157±0.04					3.6 ± 0.9	3.6 ± 0.9
81.6 ± 0.3	$(6\pm2) \times 10^{-3}$					2.9 ± 0.7	2.9 ± 0.7
78.7 ± 0.3	$(1\pm0.5)\times10^{-3}$					1.65 ± 0.4	1.65 ± 0.4
67.5 ± 0.3						< 0.06	< 0.06

Table 5

^{20}Ne	Cross sections (mb)					
E_{lab} (MeV)	^{211}At	^{210}At	^{209}At	^{208}At	^{211}Rn	^{210}(Po+At+Bi)
203 ± 4.5	23.2 ± 1				11.6 ±0.5	
201 ± 4	37.8 ± 3	26 ± 2	90 ± 3	38 ± 10	14.5 ± 1	
198 ± 4	23.2 ± 1				11.1 ±0.5	
192 ± 5						113 ± 10
188 ± 6	28 ± 1.5				12.1 ±0.6	
183 ± 6	27.7 ± 1.7				13.7 ±0.7	
178 ± 7	27.4 ± 1.4				9.7 ±0.5	
177 ± 7						134 ± 12
172 ± 8	31.2 ± 1.6				13.3 ±0.7	
161 ± 10	33.3 ± 2				13.7 ±0.8	98.6 ± 6
141 ± 12	30.4 ± 2.3				9 ± 0.5	89.6 ± 10
123 ± 14						81 ± 6
111 ± 16	24.5 ± 3				3.3 ± 0.4	41 ± 2.5
97 ± 18	3.05 ± 0.25				0.03 ± 0.03	5.1 ±0.6

Table 6

^{40}Ar	Cross sections (mb)							
$E_{(MeV)}$	^{211}At	^{210}At	^{209}At	^{208}At	^{207}At	^{211}Rn	$^{210}(Po+At+Bi)$	^{210}Po
294±6	20.6 ±2.7	20.6±4	26.5±5	9.8±1.9	1.9 ±0.6			
286±7	21.9 ±3	23.3±4.8	30.5±3.2	10.5±1.5	6.4 ±1.3	8.3 ±1.4	98 ±11	75.5±16
280±6	23.5 ±3	23.4±4.7	27 ±5.4	8 ±1.6	3.6 ±1			
272±9	23.4 ±4.3	26.5±6	29.7±3.6	16 ±2		5.72±0.9	90 ±10	63.7±16
255±10	25.4 ±3	20.3±4	23 ±4.6	7.1±1.4	2 ±0.6			
260±7 a)	24 ±2					6.2 ±2		
248±12	27.5 ±3.6	25.3±5	23.8±4.7	6.6±1.3	2.55±0.7			
241±9 a)	23 ±2.5					3.9 ±0.9		
236±13	21.8 ±3	18 ±5	15.5±3.3	< 5		3.9 ±0.6	74.7±8	56.6±13
233±5 a)	22.5 ±2.2							
226±11 a)	20.7 ±3.9							
223±15	16.6 ±2.1	11 ±2.2	6.7 ±1.3	1.55±0.33	<0.6			
221±7 a)	21 ±2.2					3.5 ±0.6		
217±16	20 ±2.7	13.3±4	12.4±2.5			1.2 ±0.25	55 ±7	41.6±11
215±4	17.5 ±1.5							
209±17	11.7 ±1.5	8.7 ±1.7	4.2 ±0.8		<0.8			
207±5	13.9 ±1.3							
206±9 a)	14.7 ±2.5							
203±6	13.6 ±1							
202±4	15.6 ±1					1.03±0.17	41.5±8	45.5±12
201±4	15.4 ±1	5.7 ±1.1					24.8±3.2	19.1±4.5
193±5	7. ±0.7							
192±7	0.48 ±0.09							
191±19	0.58 ±0.09	1.7 ±0.4	< 0.2			< 0.04	2.3 ±0.3	0.6 ± 0.6
191±7 a)	1.77 ±0.6							
190±6	1.23 ±0.15						17.9±4.3	16.9±5
186±8	0.54 ±0.07							
184±17								
182±9	0.013±0.005							
181±7	0.13 ±0.03						1.8 ±0.13	1.8 ±0.13

Table 7

^{40}Ca	Cross sections (mb)							
$E_{(MeV)}$	^{211}At	^{210}At	^{209}At	^{208}At	^{207}At	^{211}Rn	$^{210}(Po+At+Bi)$	^{210}Po
275±5	13.8 ±1.5	31.5±3	48 ±6	38 ±7	10 ±3	12.1±1.3	92 ±10	61 ±13
249±5	15.6 ±1.3	30.2±3	44.5±7	21 ±1	10.3±2.4	10 ±0.9	83 ±8	53 ±11
226±4	14.9 ±1	31.3±4	39 ±6.5	17.3±3.5	8.5 ±1.7	8.7 ±1	79 ±8	48 ±12
225±4	14.5 ±1.6	27.5±5.5	35 ±7	14.3±2.9	7.9 ±1.6	7.3 ±1.4	69 ±7	42 ±12
218±13 b)	14.2 ±1.6	33 ±3	29 ±3.5			5.1 ±0.6	69 ±7	36 ±10
214±4	11.9 ±2.5					5.7 ±1.1	51 ±5	23 ±5
213±4	7.6 ±1.2					2.2 ±0.5		
211±4 b)	3 ±0.3							
205±7	9.02 ±1.8	24.4±5	10.9±2.2			2.7 ±0.4	45.6±5	21 ±5
204±5	2.2 ±0.4					0.2 ±0.04		
204±5 b)	1.15 ±0.26							
202±5	0.53 ±0.16							
202±6	1.3 ±0.2							
199±11 b)	0.5 ±0.14	8.4±2.5	0.62±0.18	0.95±0.3				
198±6	0.17 ±0.5							
197±6 b)	0.33 ±0.4							
196±0.3 a)	1.06 ±0.1					<0.036	9.5 ±1	8 ±2
196±0.3 a)	0.95 ±0.14						10.5±2	∿10±2
195±8	1.45 ±0.24						10.8±2	∿10±2
195±6	0.37 ±0.04							
193±7 b)	0.1 ±0.04							
192±7 b)	0.28 ±0.12							
189±7	0.044±0.023							
187±7 b)	0.057±0.022						2.14±0.2	2.14±0.2
186±2 a)	0.097±0.0015							
180±9 b)	<0.009						< 1	< 1
174±7	0.003±0.0015							
174±4	<0.0037							

Table 8

^{56}Fe	Cross sections (mb)						
$E_{(MeV)}$	^{211}At	^{210}At	^{209}At	^{208}At	^{211}Rn	$^{210}(Po+At+Bi)$	^{210}Po
396±8	12 ±2					90 ±15	70 ±20
371±12	10.5 ±1.9	19.6±5	25.4±7.8	5.3 ±1.4	7.9±1.5	86 ±15	66 ±20
328±7	9.3 ±1.2	17 ±2	31 ±4	16 ±2.0	5.7±0.7	60 ±10	43 ±12
317±9	9 ±1.2	15.8±3	25.5±3.2	18.7±3	4.9±0.6	60 ±10	45 ±13
308±10	9.3 ±1.2	16.5±3	27.6±3		4.9±0.6	62 ±10	45 ±13
304±6	7.1 ±1	7 ±2	13 ±3.7	4.6±2	4.4±0.6	37 ±13	30 ±15
298±6	10.5 ±1.9	14.3±3	17.5±3.9	13.8±3.5			
291±7	7.4 ±1	9.6 ±1.2	12 ±3		1.5±0.2	27.5 ±8	18 ±9
286±8	5.9 ±0.9	1.07±0.3	2.1 ±1				
284±1	4 ±0.3					13.4 ±5	12.4±6
282±9	3.1 ±0.8					5.8 ±3	4.8±3
280±8	1.2 ±0.3	1.2 ±0.3					
276±2	1 ±0.07					2.5 ±1.2	2.5±1.2
273±10	0.4 ±0.1						
266±10	0.094±0.03						
266±4	0.055±0.03					0.95±0.5	0.95±0.5
263±11	0.013±0.006						

Table 9

^{63}Cu	Cross sections (mb)						
$E_{(MeV)}$	^{211}At	^{210}At	^{209}At	^{208}At	^{211}Rn	$^{210}(Po+At+Bi)$	^{210}Po
410±9	8.7 ±0.9	20 ±3.3	29.6±3.8	11.9±2	7.3 ±0.8	73 ±14	53 ±15
377±8	10.4 ±0.75	17.9±2.3	31.6±6	23.4±7	5.9 ±0.4	72 ±14	54 ±16
355±11	9.7 ±0.7	17 ±2.5	22.7±3.8	16.8±4.4	6.5 ±1.3	52 ±10	35 ±12
345±7	10.3 ±1	13.6±1.9	22.2±4.5	10.8±1.4			
338±7	9.4 ±1.7				4.4 ±0.8		
336±8	7.9 ±0.8	9.1 ±1.7	10.8±1.4	4.1 ±1			
328±9	5.9 ±1	9.6 ±1.5	5.8 ±1.8	1.8 ±0.5			
324±9	9.3 ±2.7						
321±16	1.53 ±0.16				0.4 ±0.04	19.4±3.2	19.4±3.2
321±10	2.84 ±0.35					22.6±3.6	22.6±3.6
317±10	3.9 ±0.7				0.68±0.12		
309±12	0.12 ±0.04					7.4 ±1.5	7.4 ±1.5
309±2[a)]	1.28 ±0.26					9.6 ±2	9.6 ±2
305±11	0.24 ±0.12						
301±13	0.017±0.008					5.8 ±1.2	5.8 ±1.2
295±3[a)]	0.03 ±0.01					1.95±0.4	1.95±0.4
289±4[a)]						0.35±0.07	0.35±0.07

Table 10

Incident ion	Energy (MeV)	Cross sections (mb)		
		^{211}At	^{211}Rn	^{210}(Po+At+Bi)
^{19}F	178 ± 6	0.092 ± 0.007	1.47 ± 0.11	27.5 ± 5.4
^{20}Ne	193.9± 5	0.15 ± 0.04	0.65 ± 0.15	
^{40}Ar	284 ± 7	0.95 ± 0.18	1.48 ± 0.37	
	262 ± 7	1.48 ± 0.14	1 ± 0.1	
	239 ±13	1.46 ± 0.24	0.60 ± 0.14	
	218 ±15	1.06 ± 0.11	-	
	197 ±15	0.8 ± 0.07	-	

Table 11

	^{210}Bi	^{210}Po	^{211}At	^{210}At		^{209}At			^{211}Rn	
	(+n,γ)	(+p,γ)	(+2p,γ)	(+2p-n,γ)	(+2p,n)	(+2p-2n,γ)	(+2p-n,n)	(+2p,2n)	(+3p-n,γ)	(+3p,n)
^{14}N	-6	6.7	1.8	-1	-5.2	-6	-8	-13.9	-3.7	-12.3
^{16}O	-11	2	4	-2.3	-3	-5.3	-9.4	-11.6	-8.2	-11.4
^{19}F	-5.8	6	2.2	-0.1	-4.8	-0.2	-7.1	-13.5	-1.8	- 5.9
^{40}Ar	-5.3	0.1	0.7	-0.8	-6.4	0.2	-7.8	-15.1	-3.5	- 8.7
^{40}Ca	-11	4	8.3	7.2	1.2	9.8	0.1	- 7.5	8.6	1.4
^{56}Fe	-6.6	1.5	3.2	1.8	-3.8	2.8	-5.2	-12.5	0.4	- 6.1
^{63}Cu	-6.2	5.1	3.6	2.6	-3.5	3.4	-4.4	-12.2	3.9	- 3

Table 12

Figure captions

Fig.1. Excitation functions for the reactions $^{14}N + ^{209}Bi \rightarrow ^{210}Po$ (squares) and ^{211}At (stars).

Fig.2. Excitation functions for the reactions $^{16}O + ^{209}Bi \rightarrow ^{210}Po$ (squares), ^{211}At (stars) and ^{210}At (points). Open symbols are from ref.10, black symbols from this work.

Fig.3. Excitation functions for the reactions $^{19}F + ^{209}Bi \rightarrow ^{210}Po$ (squares) and ^{211}At (stars).

Fig.4. Excitation functions for the reactions $^{19}F + ^{209}Bi \rightarrow ^{210}At$ (points) and ^{211}Rn (crosses).

Fig.5. Excitation functions for the reactions $^{20}Ne + ^{209}Bi \rightarrow ^{210}Po$ (squares), ^{211}At (stars) and ^{211}Rn (crosses).

Fig.6. Excitation functions for the reactions $^{40}Ar + ^{209}Bi \rightarrow ^{210}Po$ (squares), ^{211}At (stars) and ^{211}Rn (crosses).

Fig.7. Excitation functions for the reactions $^{40}Ar + ^{209}Bi \rightarrow ^{210}At$ (points), ^{209}At (black triangula), ^{208}At (circles), ^{207}At (open triangula). The dotted line represents the ^{211}At excitation function (from fig.6).

Fig.8. Excitation functions for the reactions $^{40}Ca + ^{209}Bi \rightarrow ^{210}Po$ (squares) and ^{211}At (stars). Open symbols correspond to experiments in which the purity of the Ca beam was controlled, circled symbols to experiments in which the beam energy was measured by the scattered proton technique.

Fig.9. Excitation functions for the reactions $^{40}Ca+^{209}Bi \rightarrow ^{210}At$ (points), ^{209}At (black triangula), ^{208}At (circles), ^{207}At (open triangula), ^{211}Rn (crosses). The dotted line represents the ^{211}At excitation function from fig.8.

Fig.10. Excitation functions for the reactions $^{56}Fe+^{209}Bi \rightarrow ^{210}Po$ (squares), and ^{211}At (stars).

Fig.11. Excitation functions for the reactions $^{56}Fe+^{209}Bi \rightarrow ^{210}At$ (points) and ^{209}At (triangula), ^{211}Rn (crosses). The dotted line represents the ^{211}At excitation function from fig.10.

Fig.12. Excitation functions for the reactions $^{63}Cu+^{209}Bi \rightarrow ^{210}Po$ (squares) and ^{211}At (stars). The symbols in a circle correspond to experiments in which the beam energy was measured by the scattered proton technique.

Fig.13. Excitation functions for the reactions $^{63}Cu+^{209}Bi \rightarrow ^{210}At$ (points), ^{209}At (triangula), ^{208}At (circles) and ^{211}Rn (crosses). The dotted line represents the ^{211}At excitation function from fig.12.

Fig.14. Potential energy curves for the indicated systems in the entrance channel, and after one and two-proton transfers. The sum of the coulomb and nuclear potentials is plotted versus the distance of the nucleus centers.

Fig.15. Variation of the closest distance of approach R versus the orbital angular momentum ℓ, for the indicated incident energies and for the system $^{19}F+^{209}Bi$.

Fig.16. Excitation function for the reaction $^{19}F+^{209}Bi \rightarrow ^{211}At$. The experimental points are compared with the calculated curves : dotted line = square distribution for P(ℓ) ; solid line = gaussian distribution.

Fig.17. Influence of the projectile atomic number on the cross sections for : (a) one proton, (b) two proton, (c) two charge transfer at high incident energies.

Table captions

Table 1. Decay characteristics of the observed radionucleides.

Table 2. Experimental cross sections for residual nuclei produced through $^{12}C+^{209}Bi$ reactions. The data concerning At isotopes are from ref.14.

Table 3. Experimental cross sections for residual nuclei produced through $^{14}N+^{209}Bi$ reactions.

Table 4. Experimental cross sections for residual nuclei produced through $^{16}O+^{209}Bi$ reactions.

Table 5. Experimental cross sections for residual nuclei produced through $^{19}F+^{209}Bi$ reactions.

Table 6. Experimental cross sections for residual nuclei produced through $^{20}Ne+^{209}Bi$ reactions.

Table 7. Experimental cross sections for residual nuclei produced through $^{40}Ar+^{209}Bi$ reactions.

a) Data from ref.13 after correction (see text).

Table 8. Experimental cross sections for residual nuclei produced through $^{40}Ca+^{209}Bi$ reactions.

a) Experiments in which the incident energy was measured by the scattered proton technique.

b) Experiments in which the purity of the beam was controlled.

Table 9. Experimental cross sections for residual nuclei produced through $^{56}Fe+^{209}Bi$ reactions.

Table 10. Experimental cross sections for residual nuclei produced through $^{63}Cu+^{209}Bi$ reactions.

a) Experiments in which the incident energy was measured by the scattered proton technique.

Table 11. Experimental cross sections for ^{211}At and ^{211}Rn produced through ^{19}F, ^{20}Ne and $^{40}Ar+^{205}Tl$ reactions.

Table 12. Values of the expression $Q_{gg}-\Delta B$, or $Q-\Delta B$ (MeV) for various reaction channels leading to the observed nuclei.

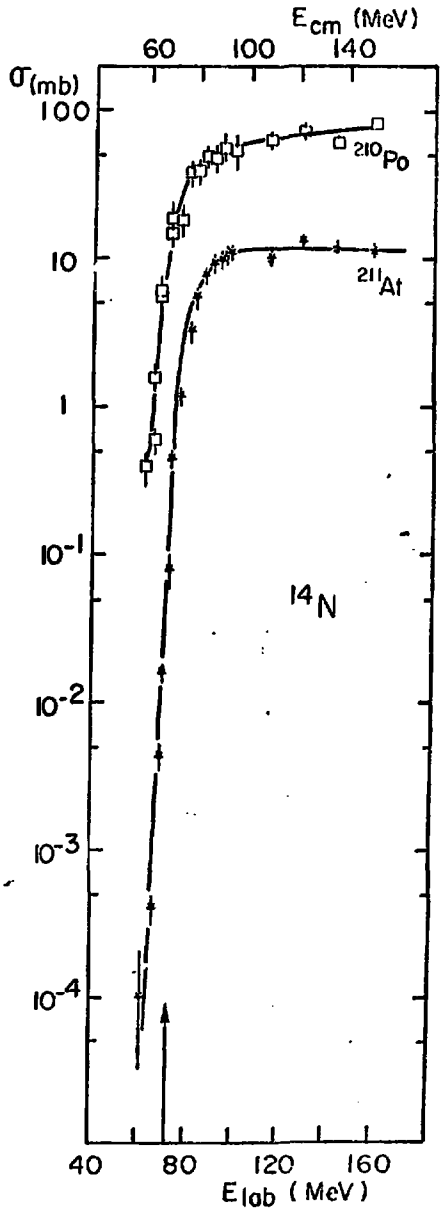
E_cm (MeV)
60
100
140
σ(mb)
100
10
1
10^-1
10^-2
10^-3
10^-4
210Po
211At
14N
40
80
120
160
E_lab (MeV)

Fig. 1.

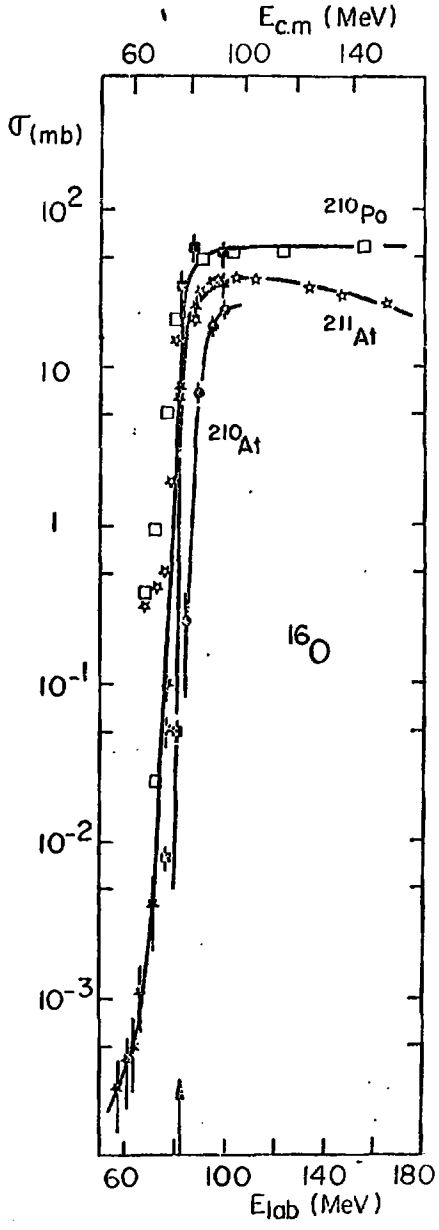
E c.m (MeV)
60
100
140
σ (mb)
10^2
10
1
10^-1
10^-2
10^-3
210Po
211At
210At
16O
60
100
140
180
E lab (MeV)

Fig. 2.

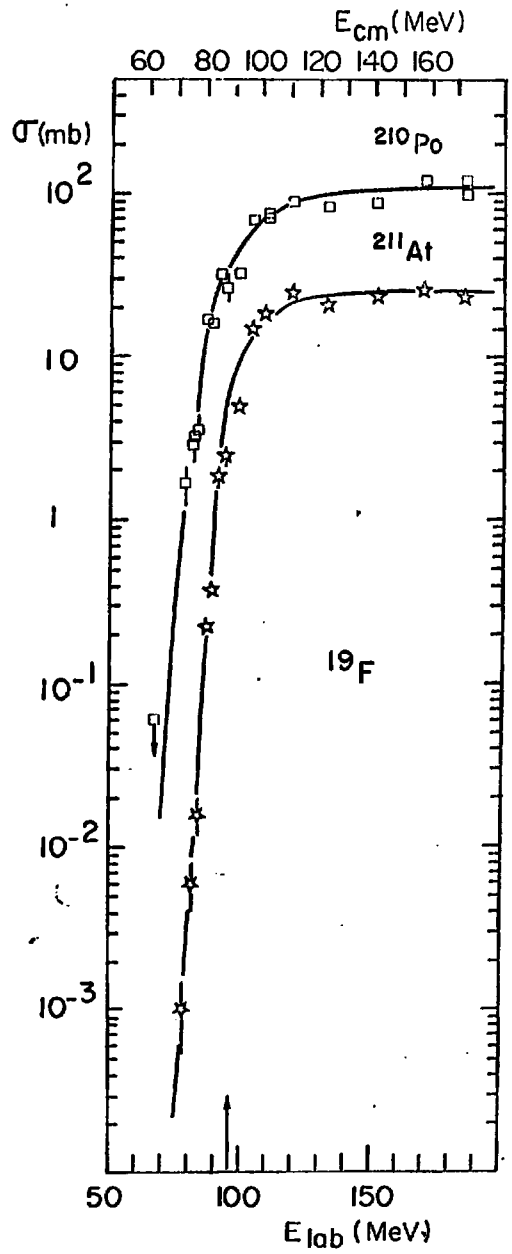
E_cm (MeV)
60 80 100 120 140 160
σ (mb)
10^2
10
1
10^-1
10^-2
10^-3
210 Po
211 At
19 F
50 100 150
E lab (MeV)

Fig. 3

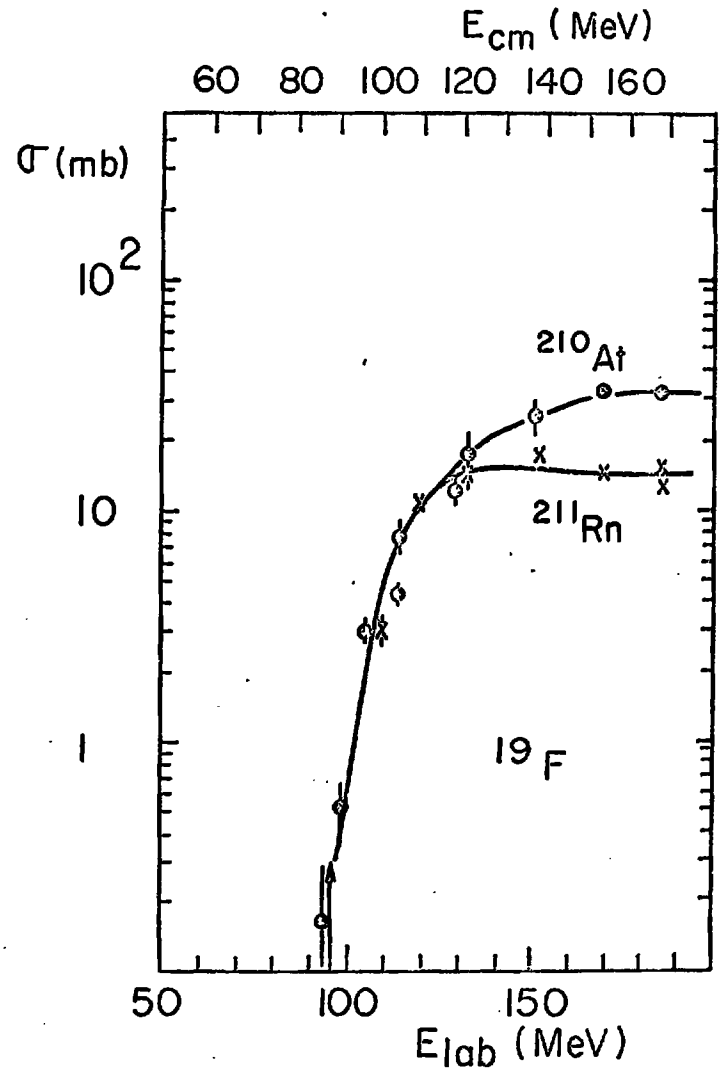
E_cm (MeV)
60 80 100 120 140 160
σ (mb)
10^2
10
1
210At
211Rn
19F
50 100 150
E_lab (MeV)

Fig. 4.

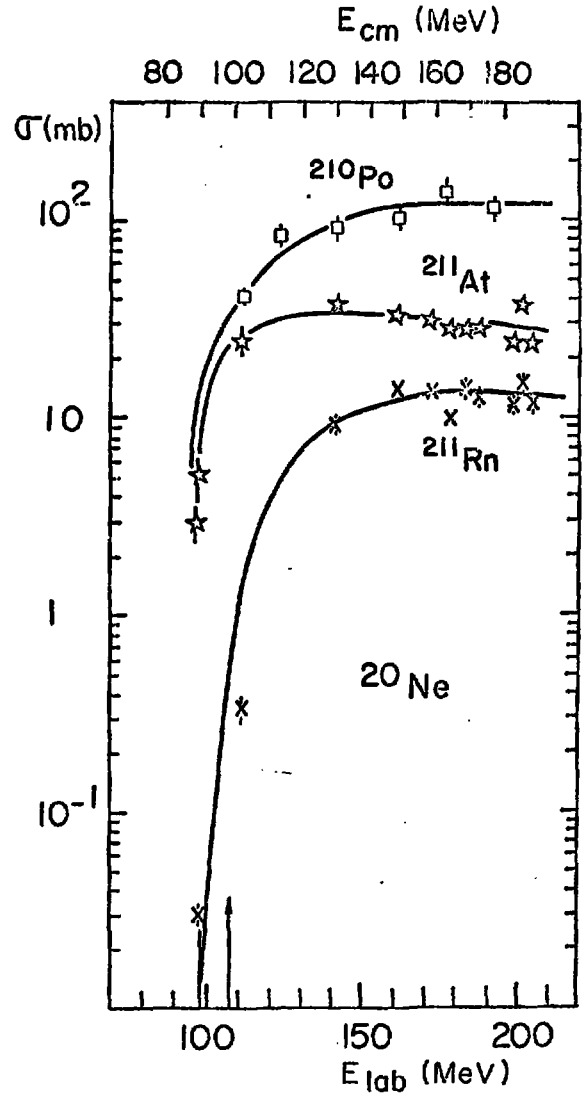
E cm (MeV)
80 100 120 140 160 180
σ(mb)
10^2
10
1
10^-1
210Po
211At
211Rn
20Ne
100 150 200
E lab (MeV)

Fig. 5.

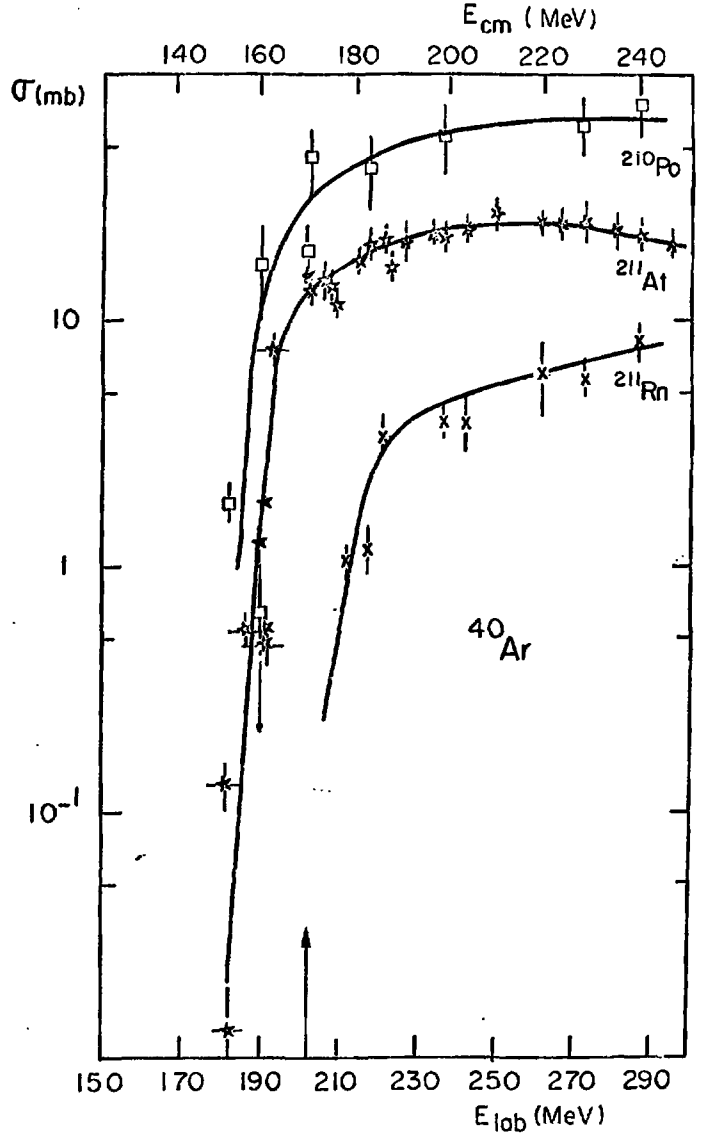
E_cm (MeV)
140
160
180
200
220
240
σ(mb)
10
1
10^-1
210Po
211At
211Rn
40Ar
150
170
190
210
230
250
270
290
E_lab (MeV)

Fig. 6

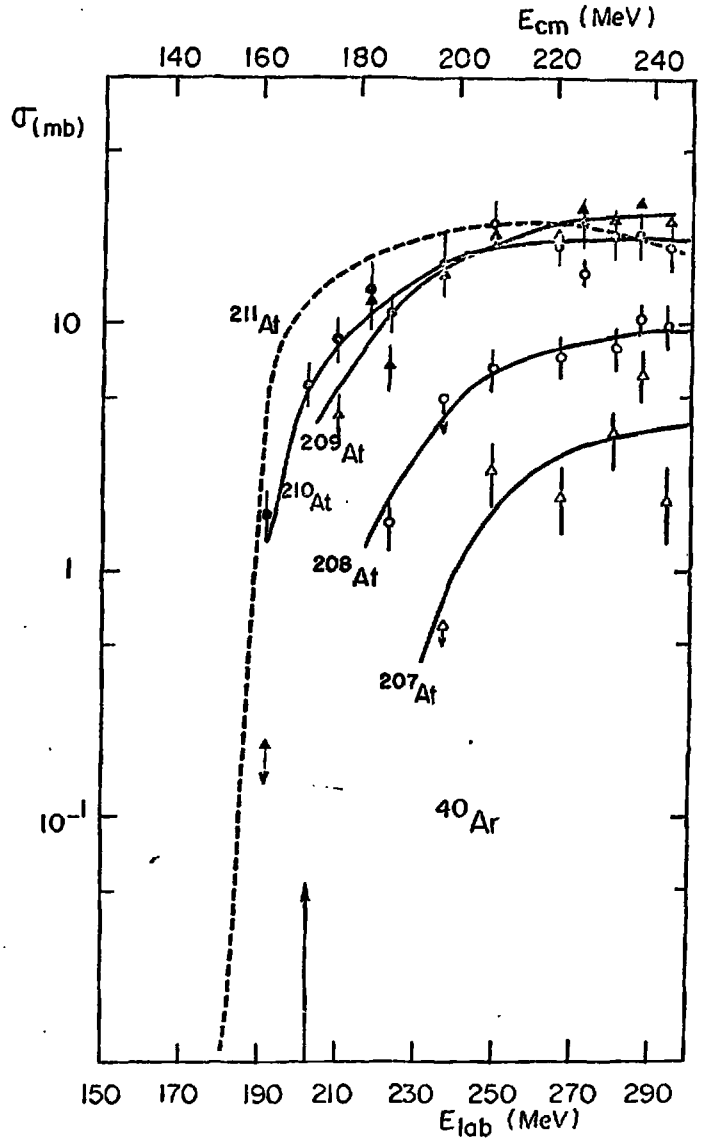
E_cm (MeV)
140
160
180
200
220
240
σ (mb)
10
1
10⁻¹
211At
209At
210At
208At
207At
40Ar
150
170
190
210
230
250
270
290
E_lab (MeV)

Fig. 7

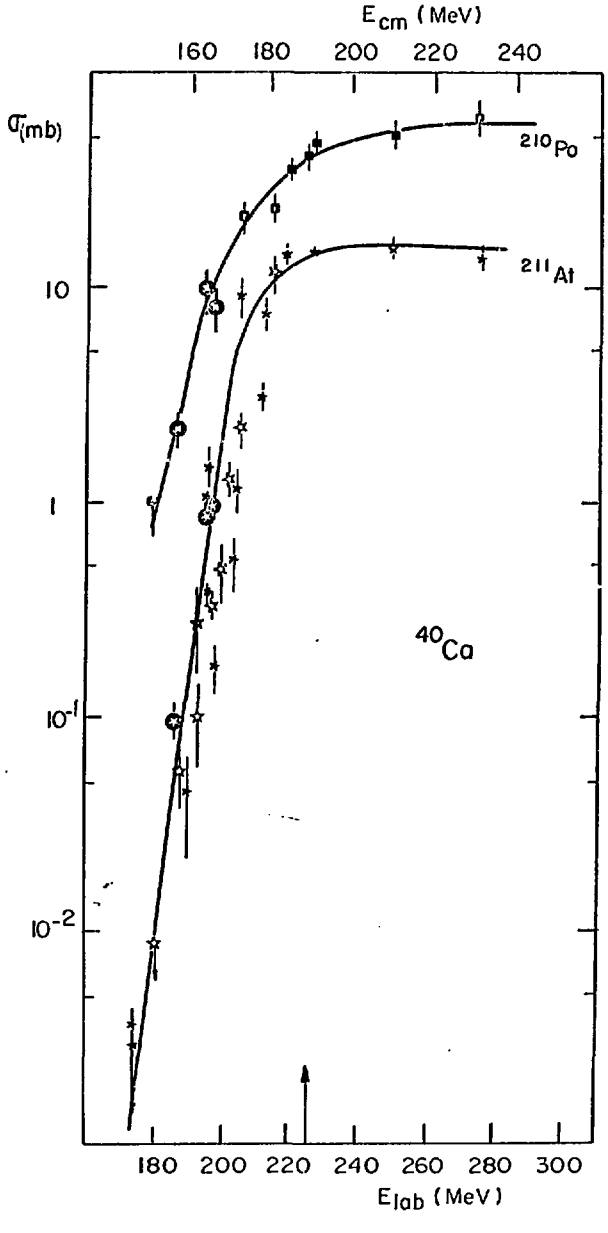
E cm (MeV)
160
180
200
220
240
σ (mb)
10
1
10-1
10-2
210Po
211At
40Ca
180
200
220
240
260
280
300
E lab (MeV)

Fig. 8.

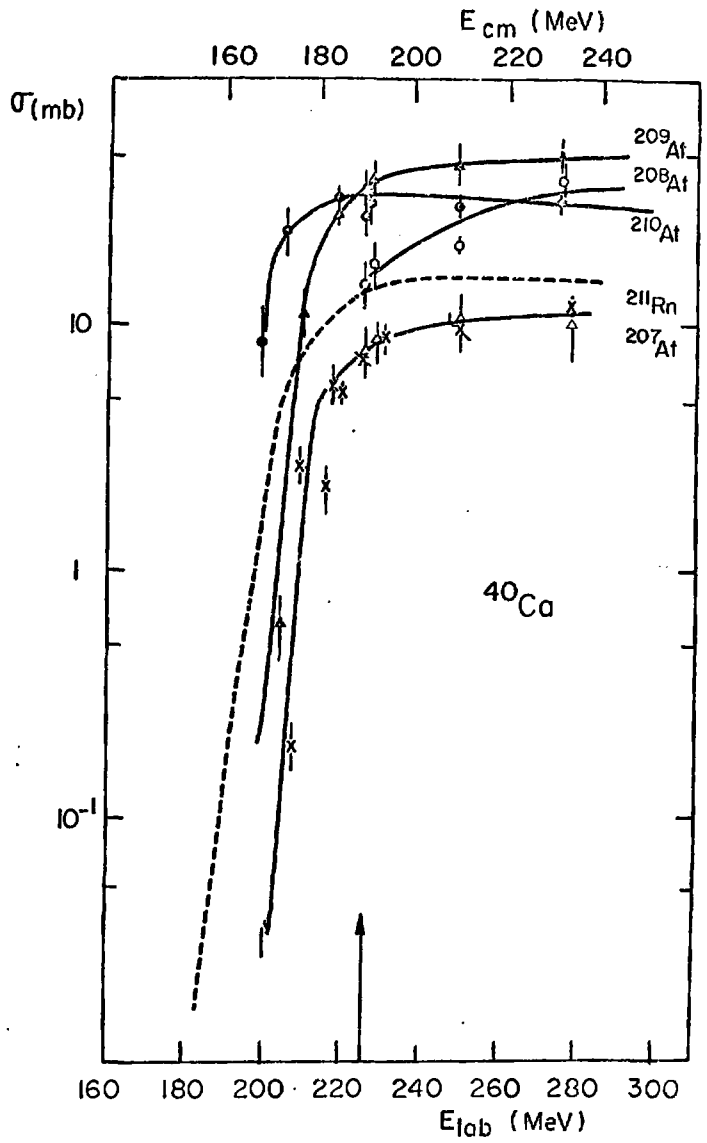
E cm (MeV)
160 180 200 220 240
σ(mb)
209At
208At
210At
211Rn
207At
10
1
10-1
40Ca
160 180 200 220 240 260 280 300
Elab (MeV)

Fig. 9

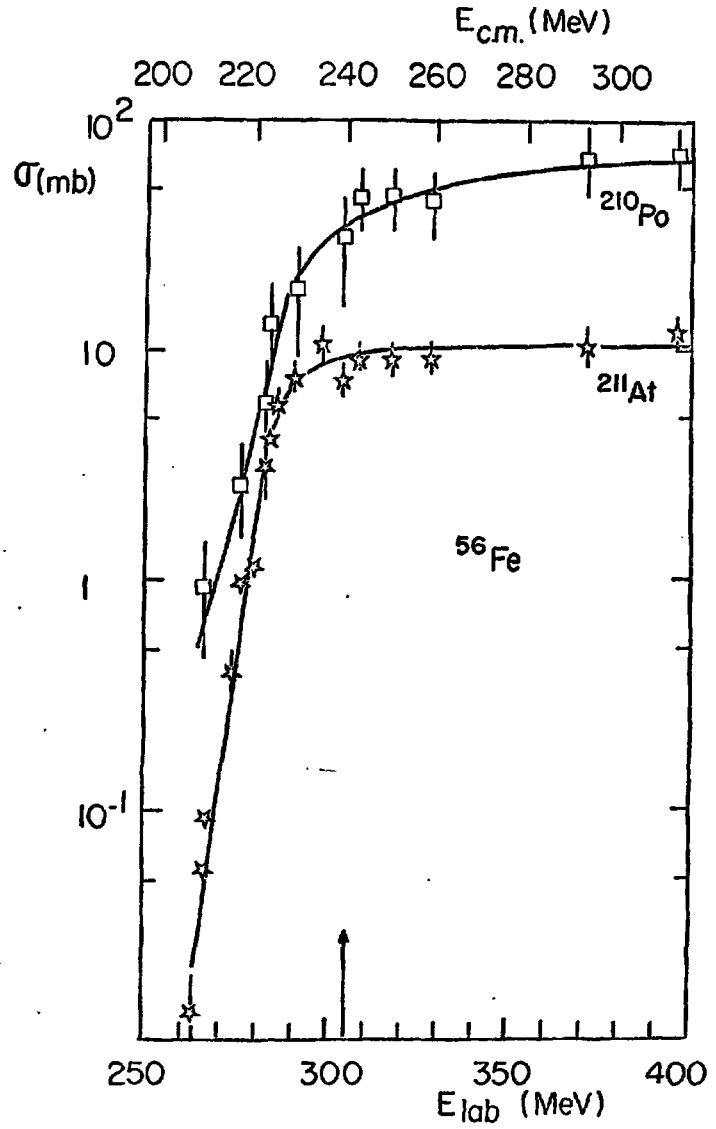
E c.m. (MeV)
200 220 240 260 280 300
10^2
σ(mb)
10
1
10^-1
210Po
211At
56Fe
250 300 350 400
E lab (MeV)

Fig. 10.

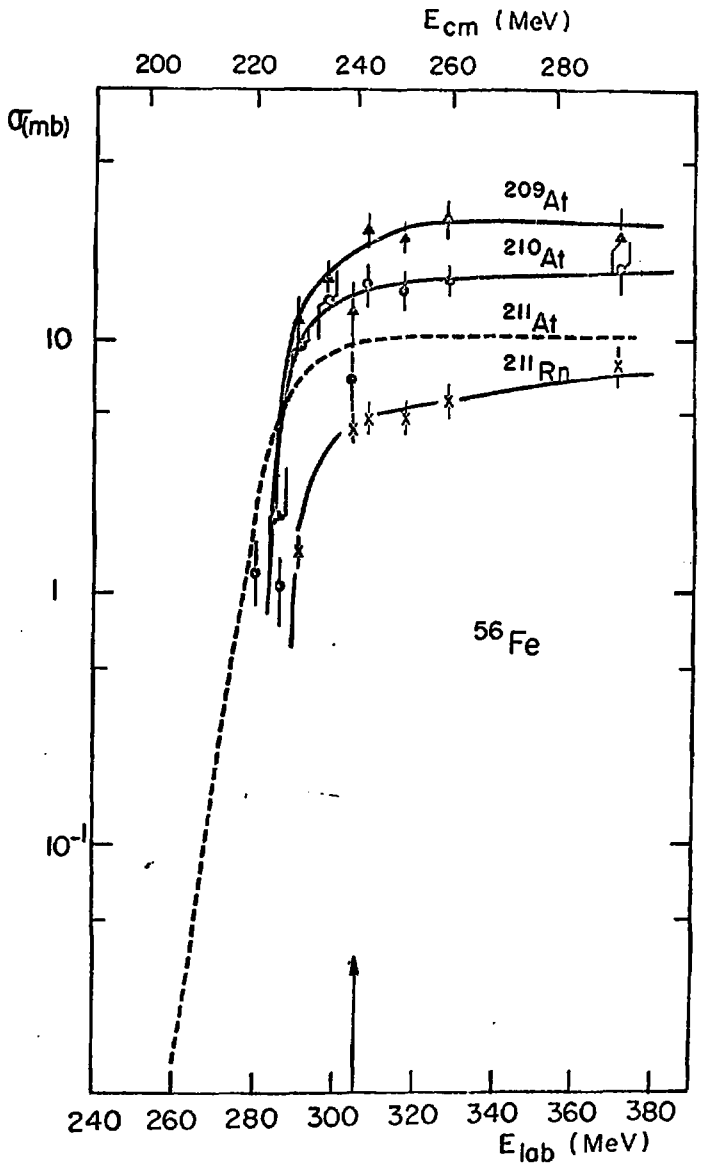
E_cm (MeV)
200
220
240
260
280
σ(mb)
10
1
10^-1
209At
210At
211At
211Rn
56Fe
240
260
280
300
320
340
360
380
E_lab (MeV)

Fig. 11.

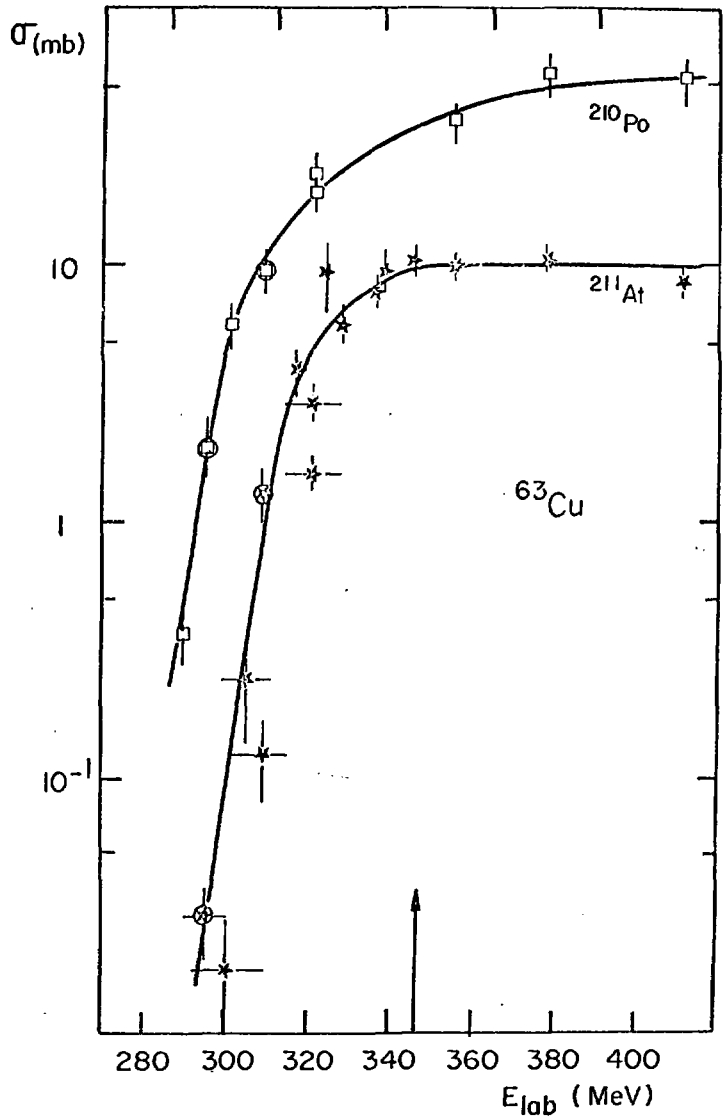
σ(mb)
10
1
10⁻¹
210Po
211At
63Cu
280
300
320
340
360
380
400
Elab (MeV)

Fig. 12.

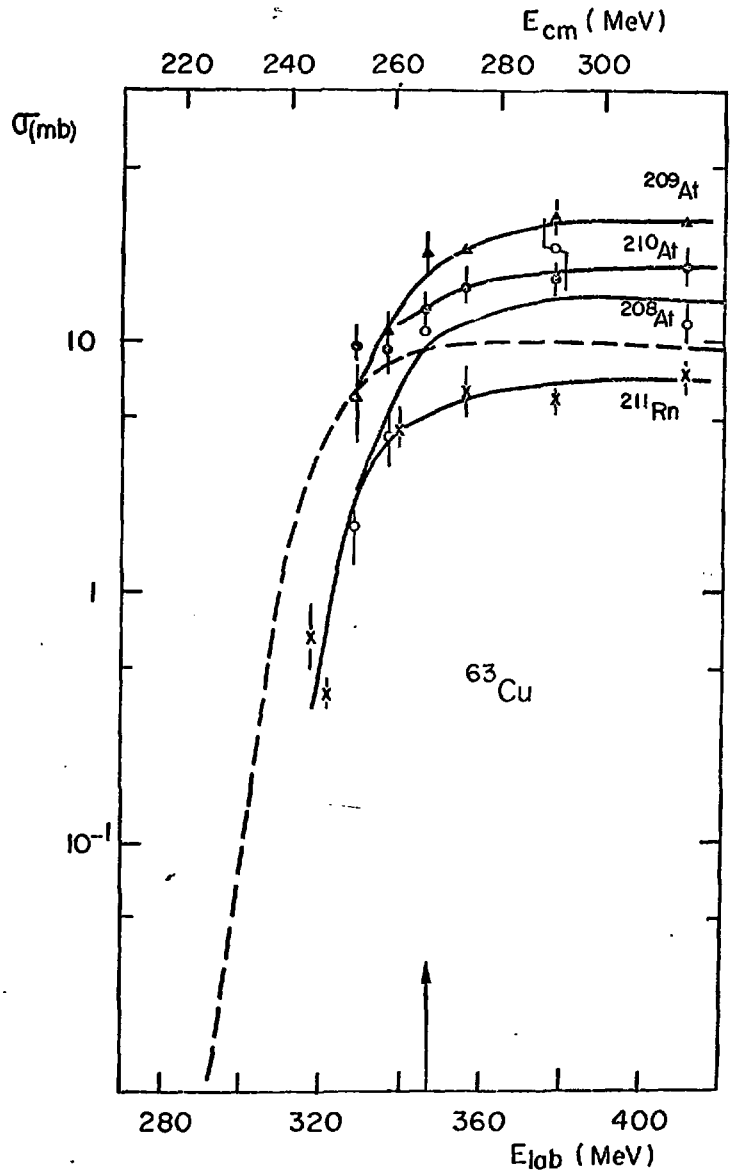
E cm (MeV)
220
240
260
280
300
σ(mb)
10
1
10⁻¹
209At
210At
208At
211Rn
63Cu
280
320
360
400
Elab (MeV)

Fig. 13.

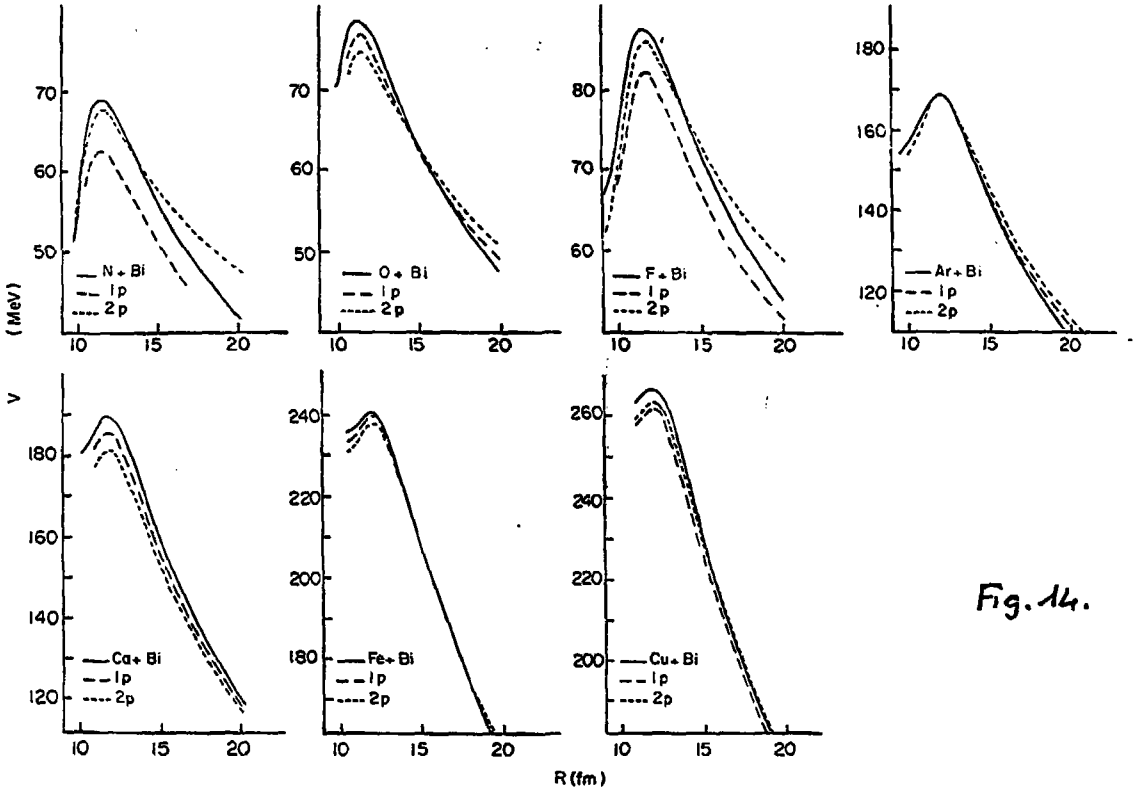

Fig. 14.

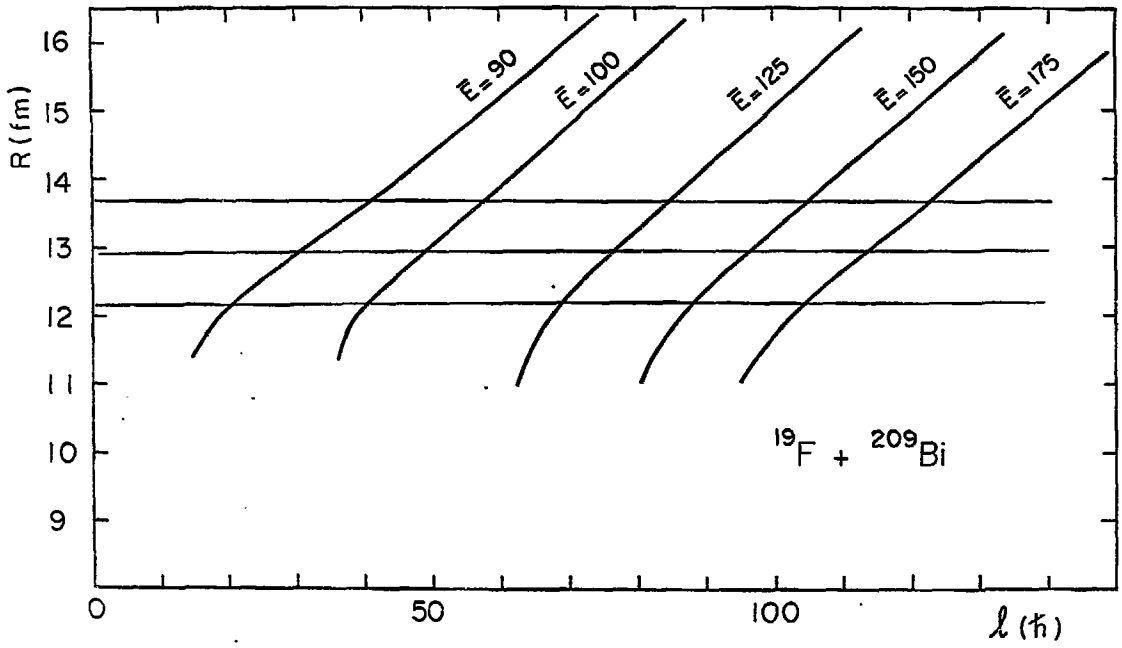
R (fm)
16
15
14
13
12
11
10
9
0
50
100
l (ħ)
E=90
E=100
E=125
E=150
E=175
19F + 209Bi

Fig. 15.

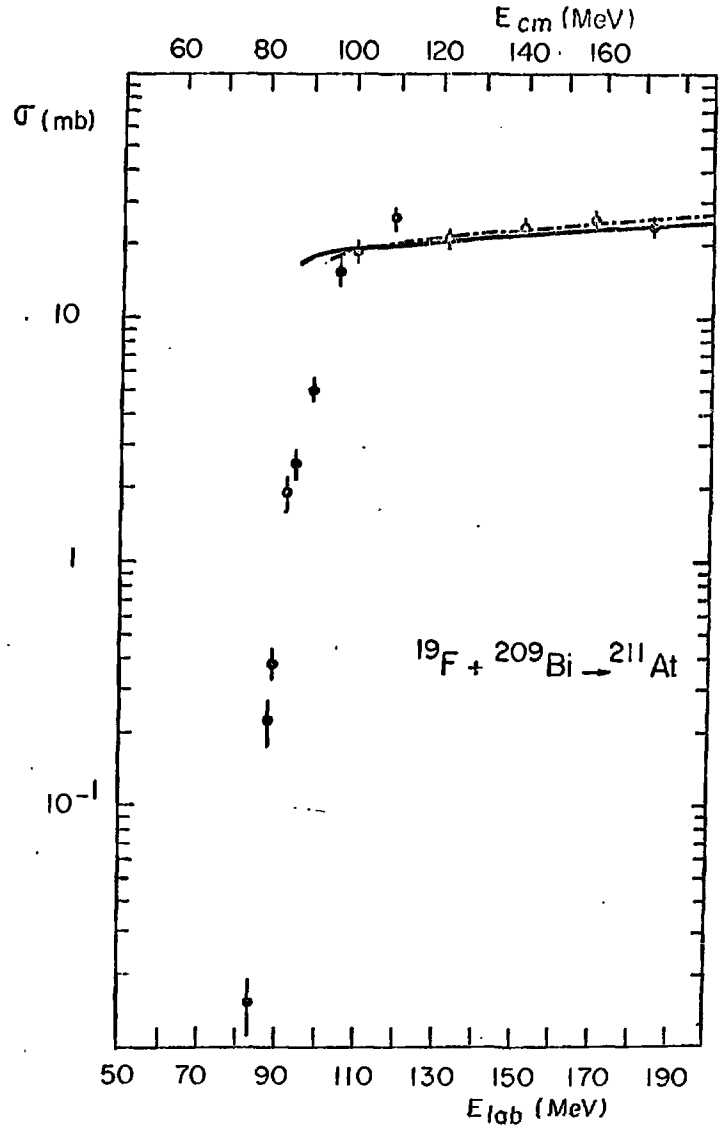
E cm (MeV)
60
80
100
120
140
160
σ (mb)
10
1
10⁻¹
19F + 209Bi → 211At
50
70
90
110
130
150
170
190
E lab (MeV)

Fig. 16.

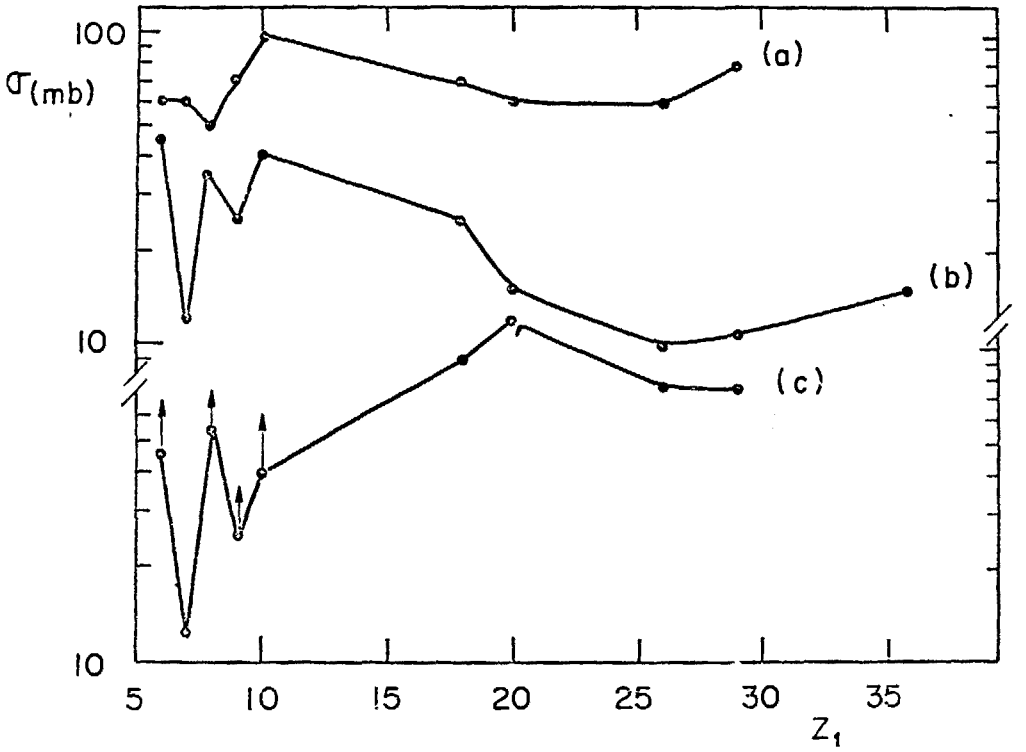

Fig. 17.